Proceedings of ASME Turbo Expo 2011
GT2011
June 6-10, 2011, Vancouver, British Columbia, Canada

GT2011-45188

EFFECT OF TURBINE AIRFOIL SHAPE ON AERODYNAMIC LOSSES FOR TURBINE AIRFOILS OPERATING UNDER TRANSONIC CONDITIONS

Santosh Abraham, Kapil Panchal, Srinath V Ekkad, Wing Ng
Department of Mechanical Engineering, Virginia Tech
Blacksburg, VA, USA

Barry J. Brown
Florida Turbine Technologies, Inc.
Jupiter, Fl, USA

Anthony Malandra
Siemens Power Generation
Orlando, Fl, USA

ABSTRACT

Profile and secondary loss correlations have been developed and improved over the years to include the induced incidence and leading edge geometry and to reflect recent trends in turbine design. All of these investigations have resulted in better understanding of the flow field in turbine passages. However, there is still insufficient data on the performance of turbine airfoils with high turning angles operating at varying incidence angles at transonic Mach numbers. The paper presents detailed aerodynamic measurements for three different turbine airfoils with similar turning angles but different aerodynamic shapes. Midspan total pressure loss, secondary flow field, and static pressure measurements on the airfoil surface in the cascades are presented and compared for the three different airfoil sets. The airfoils are designed for the same velocity triangles (inlet/exit gas angles and Mach number). Airfoil curvature and true chord are varied to change the loading vs. chord. The objective is to investigate the type of loading distribution and its effect on aerodynamic performance (pressure loss). Measurements are made at +10, 0 and -10 degree incidence angles for high turning turbine airfoils with ~127 degree turning. The cascade exit Mach numbers were varied within a range from 0.6 to 1.1. In order to attain a ratio of inlet Mach number to exit Mach number that is representative to that encountered in a real engine, the exit span is increased relative to the inlet span. This results in one end wall diverging from inlet to exit at a 13 degree angle, which simulates the required leading edge loading as seen in an engine. 3D viscous compressible CFD analysis was carried out in order to compare the results with experimentally obtained values and to further investigate the flow characteristics of the airfoils under study.

INTRODUCTION

Highly loaded airfoils are advantageous as they result in lower cost and design by reducing the number of airfoils required at each stage. However, increasing the loading could lead to an increase in secondary losses. Almost a third of the total losses in turbines are due to end wall losses. The thickness of the upstream boundary layer as well as the airfoil turning angle influences the strength of the secondary flow observed near the end walls. The secondary flow results in stagnation pressure loss which accounts for a considerable portion of the total stagnation pressure loss occurring in a turbine passage. Research on secondary flow has been prominent due to the effect it has on the turbine efficiency. However, most of these studies have been conducted at low speeds. Prakash et al. [1] studied the effect that airfoil loading has on losses at subsonic conditions. Corriveau et al. [2] analyzed the performance of aft loaded and front loaded airfoils with moderate turning angles at transonic conditions and established that aft-loaded blades yielded considerably lower losses. However, the performance of the aft loaded airfoils deteriorated at higher Mach numbers. In a similar study at low speeds, Funazaki et al. [3] found that the front loaded airfoils in their design exhibited better performance in terms of mid span losses. The works of Popovic et al. [4], and Zoric et al. [5, 6] revealed high profile loss for aft loaded airfoils and high secondary losses for front loaded airfoils. Benner et al. [7] conducted experiments at low speed on airfoils with differing leading edge geometries and concluded that the leading edge geometry has very little influence on the secondary flow. Low speed studies were conducted by Maclsaac et al. [8] to analyze the effect of turbulent Reynolds stresses in secondary flows. Jouini et al. [9, 10] investigated the flow field for transonic linear turbine cascades at design and off-design conditions, contributing to the data available on the behavior of transonic blades. The effects of varying incidence angles and Mach number on airfoil performance was studied by Abraham et al. [11] for a high turning airfoil at transonic conditions, revealing substantially higher losses at positive incidence angles and higher Mach numbers. Taremi et al. [12, 13] studied the variation of losses between low turning (90˚) and high turning (112˚) cascades and found that the high turning cascades exhibit stronger vortical structures and higher secondary flow penetration.

Performance of three airfoils at transonic flow conditions with high turning angles (~127˚) operating at varying incidences is investigated in this study. Loss systems provide predictions for pressure loss as the various geometric and aerodynamic parameters are varied. The objective of this study is to provide data at transonic conditions that can be used to confirm/refine loss predictions for the effect of various Mach numbers and gas turning. Notable recent efforts in computational fluid dynamics codes involve the work of Praisner and Clark [14, 15] and Menter et al. [16, 17]. Many researchers have previously used quasi-linear cascade design with divergent end walls, similar to the one used in the present study, in order to achieve a loading distribution similar to that of a real engine. A similar quasi 2D cascade was used by Nagel et al. [18] with the same goal in mind.

The following sections discuss experimental setup, CFD analysis and aerodynamic measurements for a transonic linear cascade with high turning angle turbine airfoils at both design as well as off-design conditions.

NOMENCLATURE

C_{ax}	Airfoil Axial Chord Length
s	Pitch
M	Isentropic Mach Number $= \sqrt{\left[\left(\frac{p_{01}}{p_{s2}}\right)^{\frac{\gamma-1}{\gamma}} - 1\right]\frac{2}{\gamma-1}}$
p_{01}	Inlet Total Pressure measured 0.45 C_{ax} upstream of the cascade
p_{02}	Exit Total Pressure
p_{s2}	Exit Static Pressure
PS	Pressure Surface
SS	Suction Surface
x	Axial Coordinate
ω	Loss coefficient $= \frac{p_{01}-p_{02}}{p_{01}-p_{s2}}$

DESCRIPTION OF THE FACILITY

A schematic of the transonic cascade wind tunnel at Virginia Tech is shown in Figure 1. The wind tunnel is a blow down facility capable of a twenty second run time. The air supply is pressurized by a four-stage Ingersoll-Rand compressor and stored in large outdoor tanks. The maximum tank pressure used for transonic tests is about 2068 kPa (300psig). A control valve is used to regulate the flow from the tanks to the test section. During a run, the upstream total pressure is held constant by varying the opening of a butterfly valve controlled by a computerized feedback circuit. Steady flow is maintained in the cascade for the duration of the data acquisition. There is additionally a safety valve upstream of the control valve to start and stop the tunnel. The airfoil isentropic exit Mach number is varied by changing the upstream total pressure.

The cascade, as shown in Figure 2, consists of 6 airfoils resulting in 5 passages, with controlled bleed flow above the first airfoil. The airfoils are mounted on a rotatable window, which allows for changes in incidence angles as and when required. Airfoil 3 is considered as the center airfoil and is instrumented to measure the static pressure at midspan. Airfoil 2 is instrumented on the pressure side and Airfoil 4 is instrumented on the suction side for midspan static pressure measurements to ensure flow periodicity in the two passages adjacent to the center airfoil. In order to ensure good flow periodicity it is essential that the stagnation streamlines for the outer airfoils of the cascade are identical. A headboard, positioned upstream of the cascade is instrumental in controlling the incoming flow by preventing an induced incidence angle effect on the leading edges of the airfoils. The headboard is used to create and control a flow bleed that prevents the flow from turning prior to reaching the leading edge of the airfoils. Good inlet flow conditions can be achieved by careful adjustment of the headboard angle which aids in maintaining uniform and periodic flow through each airfoil passage and ensuring that the flow angle gradient ahead of the cascade is zero. A slot located 0.45 C_{ax} upstream of the cascade is used to measure the turbulence and velocity distribution at the inlet of the cascade. It is also used to measure inlet total pressure at midspan which is used as a reference total pressure for isentropic Mach number calculation. Tailboards are positioned at the top airfoil and bottom airfoil trailing edges to help guide the flow.

The exit span is increased relative to the inlet span resulting in one end wall diverging from inlet to exit at a 13 degree angle. The purpose behind this is to obtain a ratio of inlet Mach number to exit Mach number that is representative to that encountered in a real engine and also to simulate the required realistic leading edge loading in a quasi 2-D cascade. The airfoil span increases by about 16% linearly in the axial direction from inlet to exit of the cascade.

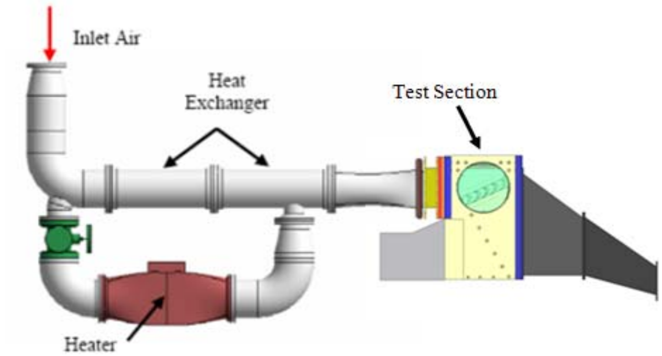

Figure 1 : Virginia Tech transonic cascade wind tunnel

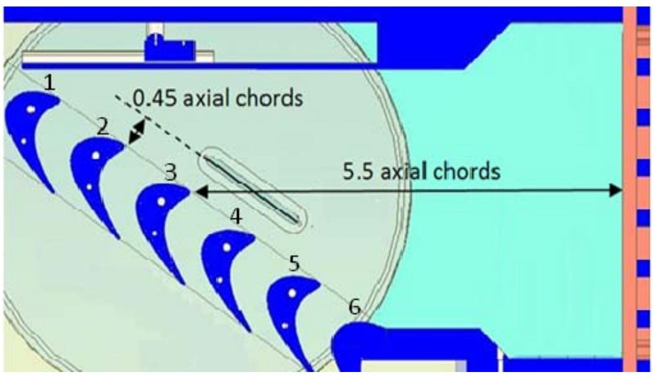

Figure 2 : Cascade diagram showing the airfoils and the axis orientation for measurements with the traverse

INSTRUMENTATION AND DATA ACQUISITION

Inlet Flow Measurements

A turbulence grid is placed 5.5 upstream of the cascade as shown in Figure 2 to obtain the desired level of turbulence. Aerodynamic measurements were made on a plane 0.45 upstream of the airfoil leading edge. The measurements covered one and a half airfoil pitches and extended from midspan to near the endwall. A pitot probe was used to measure the inlet velocities at midspan and also to estimate the boundary layer thickness. Pitchwise traverse measurements were made to establish the uniformity of incoming flow. A single wire hot-wire probe was employed to measure the inlet free stream turbulence intensity based on an isotropic turbulence assumption.

Static Pressure Measurements

The center airfoil and the two adjacent airfoils were instrumented with pressure taps placed at the midspan. In order to estimate the inlet and exit Mach numbers, static pressure taps were positioned on the end walls of the cascade on a plane 0.5 upstream of the airfoil leading edges and 0.5 downstream of the airfoil trailing edges.

Loss coefficient measurements

The loss coefficient measurements were carried out at 1.0 axial chord downstream from the airfoil trailing edge. A Kiel probe was used to capture the velocity profiles in both the spanwise as well as in the pitchwise direction. The spanwise area averaged loss coefficient was measured at 11 different spanwise locations during multiple runs, from midspan to the inclined endwall for the design exit Mach number and the design incidence angle for all the airfoil geometries. The pitchwise area averaged loss coefficient was measured at midspan for Mach numbers varying from 0.6 to 1.1 and for incidence angles -10, 0 and +10 for all three airfoil geometries.

CFD ANALYSIS

Computational fluid dynamic analysis has become a standard tool today to assist the understanding of flow behavior obtained from experimental results. Numerical investigations were carried out for all three blades being studied using a commercial three dimensional viscous CFD code. The airfoil mid-span blade loading results and the pitch-averaged loss coefficient profiles one axial chord downstream of the trailing edge were compared with the experimental results in order to validate the results of CFD analysis. These CFD predictions were used to further assist the analysis of flow behavior in combination with experimental results.

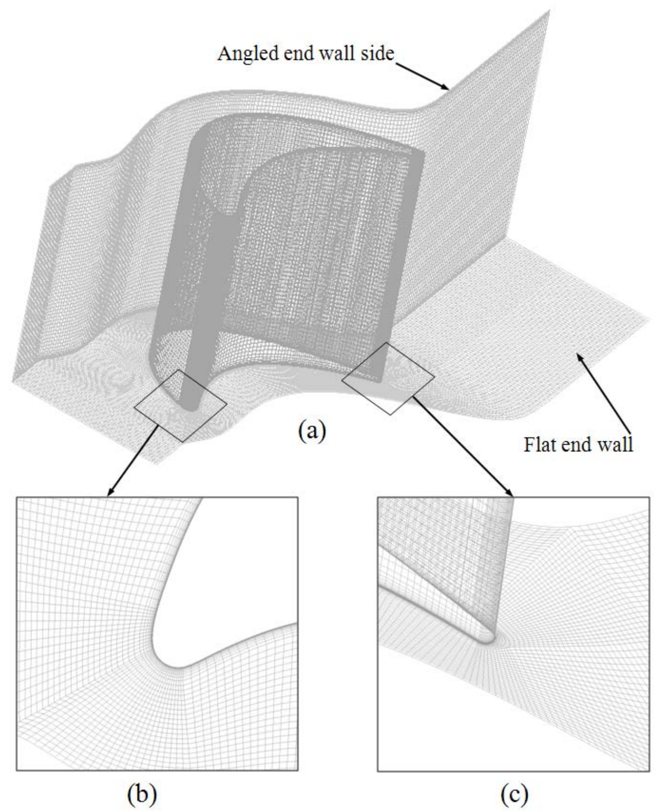

Figure 3: (a) Computational grid (b) Enlarged mesh region near blade leading edge and (c) enlarged mesh region near blade trailing edge

Computational Geometry and Grid

The computational domain for blade A is shown in Figure 3 and Figure 4. As shown in Figure 4, the domain consists of a blade profile and two periodic curves one pitch apart. Hence, the domain represents one passage of a linear turbine cascade used for the experiments. The inlet to the domain is 0.5 axial chord upstream of the blade leading edge and the exit channel is extended 1.5 C_{ax} downstream of the blade trailing edge. The passage has one angled end wall diverging from the axial leading edge of the blade up to the axial trailing edge and one flat end wall as in the experimental setup.

The mesh used was selected after a mesh refinement study. The mesh uses geometric clustering near the end walls and blade surface in order to simulate the boundary layer. This node-clustering results in y+ values less than 1 for most of the domain except a very small region near the trailing edge where it is close to 2. This baseline mesh along with one coarser and one finer mesh were used for a mesh refinement study.

Based on the mesh refinement study results and computational time considerations, the baseline mesh was selected for further study. Similar mesh densities were used for all the blades. Details of the mesh refinement study are given in the ensuing discussion.

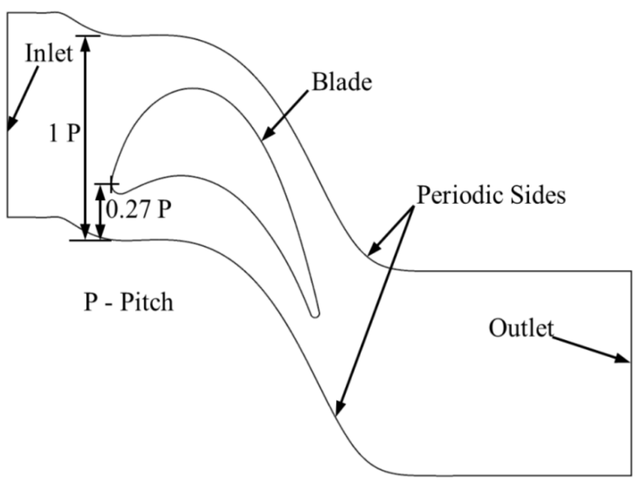

Figure 4: Computational domain and boundaries

Computational Model and Boundary Conditions

Various boundary conditions applied on the model are as shown in Figure 4. The experimentally measured inlet total pressure profile was applied at the inlet boundary and a uniform total temperature was specified. Because of the high turning encountered by the flow within the blade passage, the flow angle near the blade leading edge reduces as compared to that specified at the inlet boundary 0.5 Cax upstream. This flow angle change near the blade leading edge is called the induced incidence angle effect. Hence a flow direction with a slightly positive incidence angle was specified at the channel inlet so that the flow near the blade is at the design angle. After each simulation, it was confirmed that the flow close to the blade leading edge is at the required angle. The mass flow averaged angle 4mm in front of the airfoil axial leading edge is considered the design flow angle.

A prescribed average static pressure condition was specified at the outlet boundaries. Side walls were given a translational periodicity boundary condition. Passage end walls and the airfoil surface were specified to be adiabatic walls with zero slip velocity. Based on the past experience from similar aerodynamic simulations, the SST-k ω turbulence model was used. Convergence criterion for the RMS residuals was chosen to be 5×10^{-5} based on the mesh refinement study.

The CFD solver produced airfoil loading results, that are in reasonably good agreement with the experimental results as discussed in the 'Results' section. In addition to the blade loading, the total pressure loss profile 1 Cax downstream of the axial trailing edge was also studied. The profiles, as shown in Figure 12, are obtained by passing a curve through pitch-averaged values of loss coefficients calculated at many spanwise locations from the angled end wall up to the mid-span. It was observed that the change in inlet total pressure profile, turbulence model, consideration for transitional turbulence and grid size had less influence on the loss profile predictions as compared to the change in advection scheme used for the calculations. The CFD solver offered three choices: (1) first order upwind (2) second order high resolution scheme and (3) a combination of the two by using a blend factor value ranging from 0 for the upwind scheme to 1 for the high resolution scheme. It was observed that the second order high resolution scheme does not show enough mixing and hence results in a considerable under-prediction of losses 1 Cax downstream. The advection scheme with a blend factor of 0.1 showed a reasonably good agreement with the loss profiles, especially for blade A and C. Although not discussed in this study, experimental measurements of the losses were also carried out on a 2D plane 0.1 Cax downstream for blade A. The blend factor scheme results showed a good agreement with pitch-averaged loss profiles as compared to the high-resolution scheme. The change in blade loading for the three schemes was small. Hence, the authors believe that one should use an appropriate scheme and blend factor value depending upon the purpose of analysis and prediction and the uncertainty in experimental results. Additionally, it was observed that the required blend factor value remained the same for all the three blade profiles and different Mach numbers as long as the incidence angle was kept the same. For different incidence angles, however, the blend factor value needs to be changed. The loss profiles shown in Figure 12 were obtained using a blend factor value of 0.1. The flow structures shown in Figure 7 are those obtained using the high resolution scheme to ensure that same scheme is used to enable comparison between the results. The flow structures for the high resolution scheme and those for the blend factor scheme were compared for blade A at the design incidence angle and were found to be qualitatively similar.

Mesh refinement study

Three different grids as described in Table 1 were used for the mesh refinement study. A baseline mesh with one coarser and one finer mesh with a uniform mesh refinement factor of 1.5 over the whole domain were used. Maximum possible edge length for any cell was restricted to be 2.2 mm. Near-wall clustering was selected such that y^+ values remain below 1 for the fine and baseline meshes and very close to 1 for the coarse mesh.

All the meshes used were generated using an identical blocking strategy, which resulted in a very high quality mesh with minimum mesh quality of 0.5 for all the cells. All the meshes had a very high value of cell orthogonality with more than 92% of the cells having an orthogonality angle greater than 62^{o}.

Table 1: Mesh information

Mesh	Number of nodes
Coarse	591468
Baseline	1812030
Fine	6559938

Mass averaged loss coefficients at 0.5 C_{ax} and 1.0 C_{ax} downstream of the trailing edge were used for calculation of observed order of accuracy. In order to simulate exact solution of discretized equations required for discretization error estimate, a simulation with RMS residuals of 1×10^{-12} at convergence was used. The observed order of accuracy was found to be 1.37 using Richardson extrapolation method. Based on this observed order the magnitude of discretization error in the value of loss coefficients was found to be about 6.5% at the design conditions. The shape of the pitch-averaged loss profiles 1 Cax downstream of the axial trailing edge did not show any significant difference for all three meshes and hence the spanwise mesh resolution can be considered sufficiently small.

AIRFOIL GEOMETRIES

While this paper contains several discussions of airfoil flow physics and fluid mechanics, the main focus of this research was to analyze and compare the aerodynamic performance of three turbine airfoil designs. The three airfoils being studied here are high turning transonic airfoils with identical flow angles and the same axial chord length. Therefore the Zweifel coefficient, given by equation 1 would be the same for all three airfoils. The airfoils are designed for the same velocity triangles (inlet/exit gas angles and Mach number). Airfoil curvature and true chord are varied to change the variation in loading vs. chord. The goal is to see if a given type of loading distribution results in better performance.

$$Z = 2\frac{s}{C_{ax}}\cos^2\beta_2(tan\beta_1 - tan\beta_2) \qquad (1)$$

Airfoil suction surface curvature and channel area distribution versus chord are varied to create differences in chordwise distribution of airfoil loading and suction surface diffusion for the candidate airfoil designs. Details of the procedure and design philosophy used are proprietary. It is advantageous to reduce the number of airfoils to the maximum possible extent since each individual airfoil adds to the overall weight and expense. With the added features such as special materials using expensive manufacturing processes and cooled airfoils with complex internal flow passages, reduction of the number of airfoils is important. The Zweifel coefficient, an aerodynamic loading index of a cascade, provides a reliable and basic method for making an initial estimate of the minimum solidity and number of required airfoils. Investigations of the midspan surface loading profile, profile losses, spanwise losses and area averaged total losses were conducted to determine the performance characteristics for the airfoil designs.

The stagger angle and the unguided turning angle are fundamental parameters that affect the loading distribution. The stagger angle is the angle between the line joining the leading and trailing edge of the airfoil to the engine axial direction. The unguided turning angle is the amount of turning that the fluid undergoes over the rear section of the airfoil extending from the airfoil throat to the trailing edge. The unguided turning angle for blade B is the highest and that for blade C is the lowest while the stagger angle is almost the same for all three airfoils.

RESULTS AND DISCUSSIONS

Inlet Flow Measurements

It is essential for CFD calculations to have an accurate inlet boundary layer profile. Aerodynamic inlet spanwise measurements on a plane 0.45 axial chord upstream of the airfoil leading edge plane revealed that the inlet flow had about an 11 mm thick boundary layer from the end wall. The inlet flow profile obtained from the experiment was used in the CFD calculations. The primary measurement passage measured an isotropic turbulence intensity level of 8%. It is worth mentioning here that Gregory-Smith and Cleak [19] studied the influence of inlet turbulence intensity on secondary flows and concluded that it had very little influence on the flow field and loss behavior. The upstream flow uniformity was established with a maximum deviation of ±0.4%.

Static Pressure Measurements

The surface isentropic Mach number was calculated using the measured airfoil surface static pressure at midspan and upstream total pressure of the cascade. The uncertainty was established at ±0.1%. The periodicity of flow through the passages was satisfactory and was established for all the cases that were studied using midspan pressure taps on the center airfoil and its adjacent airfoils. The local Mach number distribution on the three airfoil surfaces were measured for varying exit Mach numbers at 3 different incidence angles. Figure 5 shows the comparison of midspan airfoil loading between experimental values and CFD analysis results at 0 degree incidence and design Mach number for the airfoils. It can be seen that there is a good agreement between experiments and CFD analysis. The experimental and CFD loading on the airfoils were validated at design Mach number and design incidence angle for the cases studied. Additionally, a case with -10 deg incidence angle and design Mach number is also shown for airfoil A. A good agreement between the CFD results and experimental results even at off design conditions is evident.

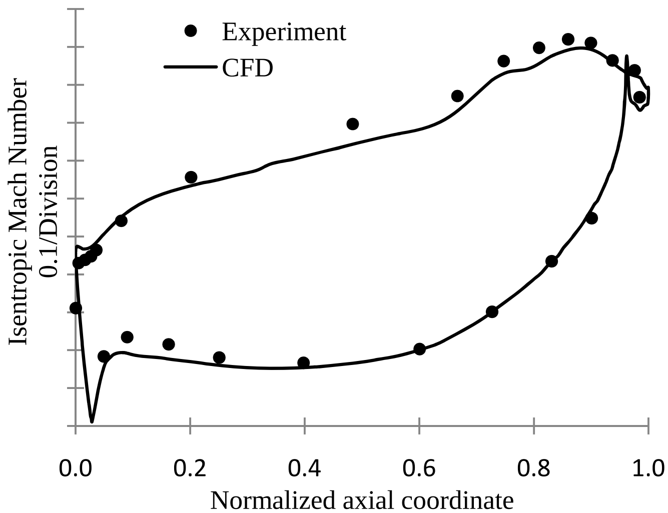

(a)

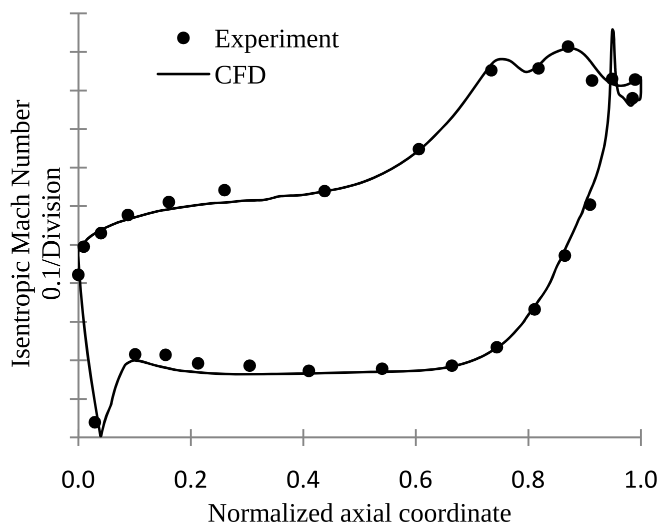

(b)

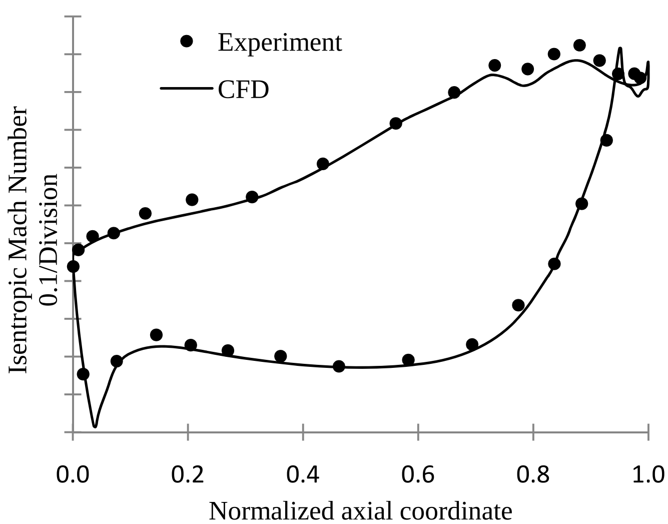

(c)

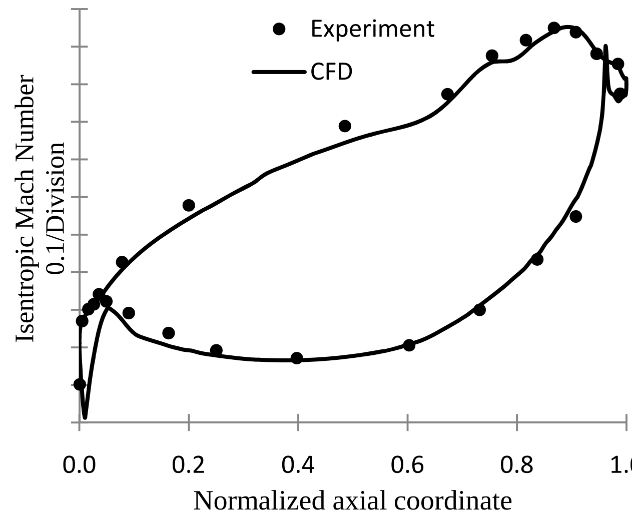

(d)

Figure 5: Comparison of midspan airfoil loading from CFD analysis and experiments at design Mach number for (a) airfoil A at design incidence angle (b) airfoil B at design incidence angle (c) airfoil C at design incidence angle (d) airfoil A at -10 degree incidence angle

Figure 6 shows the loading on the airfoils at design conditions. The loading is relatively higher around midchord for airfoil A than for airfoils B and C due to axial redistribution of loading. The loading differences were by design from changes in airfoil shape and curvature. It is apparent that airfoil B is comparatively more aft loaded. The unguided turning for airfoil B is the highest. Compared to airfoil A, airfoil B reveals a considerable amount of aft diffusion which will result in higher profile losses downstream. The profile losses resulting from different airfoil loadings are studied in detail in further sections.

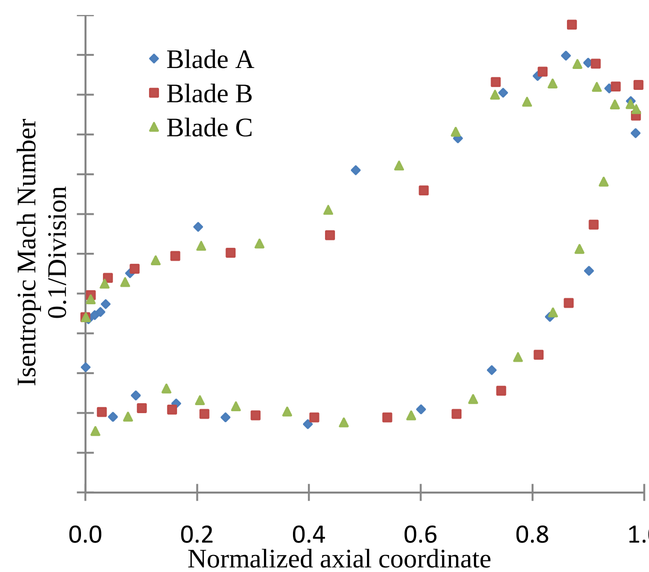

Figure 6: Loading distribution on the three airfoils

The swirling strength plots for 0 degree and +10 degree incidence angles obtained from CFD analysis for Airfoil A are shown in Figure 7 (a) and 7 (b) respectively. Swirling strength is defined as the discriminant of velocity gradient tensor for complex eigenvalues. The swirling strength isosurface indicates local swirling flow pattern. Existence of large secondary flow field for +10 degree incidence as compared to moderate secondary flow structure for 0 degree incidence angle suggests higher loss for +10 degree incidence angle as compared to design conditions.

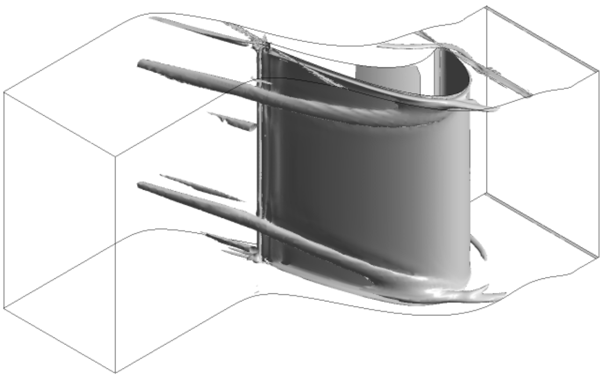

Figure 7: (a) Swirling strength Isosurface for 0 degree incidence for Blade A

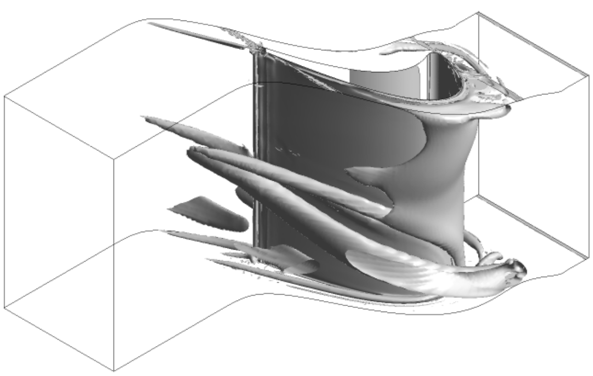

Figure 7: (b) Swirling strength Isosurface for +10 degree incidence for Blade A

Figures 8, 9 and 10 show the effect of Mach number variation, obtained from experiments, on the airfoil loading for the three airfoils at design incidence angle as well as for the two off-design incidence angles. As the positive incidence increases to + 10 degrees a strong suction peak develops on the suction side near the leading edge and as the incidence angle reduces to -10 degrees the leading edge loading considerably decreases. In other words the loading on the three airfoils change from aft loading for the -10 degree incidence angle cases to front loading for the +10 degree incidence angle cases. For all cases there is no significant change on the pressure side loading, up to near trailing edge, with varying exit Mach numbers. For all higher exit Mach number cases (> 0.9) the loading on the suction side remains relatively the same from leading edge to 0.7 normalized axial coordinate as the exit Mach number increases. This can be attributed to the choking of the flow in the blade passage. For the +10 degree incidence angle cases for all three airfoils, a mild deceleration is noticeable on the suction surface from the leading edge to mid-chord. As a result the suction side boundary layer will tend to be thicker for these cases as compared to the other two cases, which will result in higher losses for these cases.

At higher exit Mach numbers a normal shock impinges on the suction side and as the Mach number increases further, the shock becomes sharper and migrates more towards the trailing edge for all cases tested. Note that while all airfoils experience the shock at higher Mach numbers, the magnitude of the resulting pressure gradient (velocity drop) as a function of the exit Mach number and the rate at which the shock appears and grows vary between the three airfoil designs. The shocks are less prominent on airfoil A which would result in the other airfoils showing higher losses due to the shock effect.

Loss coefficient measurements 1.0 axial chord downstream:

Profile Losses:

Profile losses are associated with boundary layer growth over the blade profile and include separation loss under adverse conditions of extreme turning angles or high inlet Mach numbers. Shocks/ boundary layer interactions also contribute to profile losses. The pitchwise area averaged loss coefficients are measured 1.0 axial chord downstream from the trailing edge of the cascade using a traversing kiel probe at midspan at the different incidence angles and varying exit Mach numbers and are represented in Fig 11. Measurements are made at a total of 60 points during each run, across a distance of pitch length*1.67. From the analysis of the airfoil loading we concluded that airfoil B showed a significant amount of aft diffusion as compared to airfoil A, which therefore results in higher profile losses for airfoil B. The term aft diffusion refers to the static pressure rise or the drop in Mach number from the peak location to the trailing edge. When the aft diffusion becomes excessive, flow separation on the suction surface occurs, which results in high losses. Aft diffusion decreases as the loading moves forward, as in the case of Blade A. Airfoil C is also more aft loaded than airfoil A. Another factor that ensures lower losses for airfoil A is the fact that the oblique shocks originating at the trailing edge of the adjacent airfoil and impinging on the rear of the suction surface on airfoil A at higher Mach numbers are considerably less than those on the other two airfoils. This will favorably affect the losses. The flow diffuses only once along the aft section of the suction side of airfoil A as compared to the multiple acceleration and diffusion processes on the aft portion of airfoils B and C. For the design incidence angle cases as well as for the -10 degree incidence angle cases, airfoil C sees the strongest shock and corresponding drop in Mach number (Figure 10 a, b). This in turn increases the direct total pressure losses through the shock wave. The aft diffusion for these two incidence angle cases seems to be more prominent for airfoil C which also directly influences the total pressure downstream of the cascade. These factors make the losses for airfoil C more prominent at zero incidence and negative incidence angles.

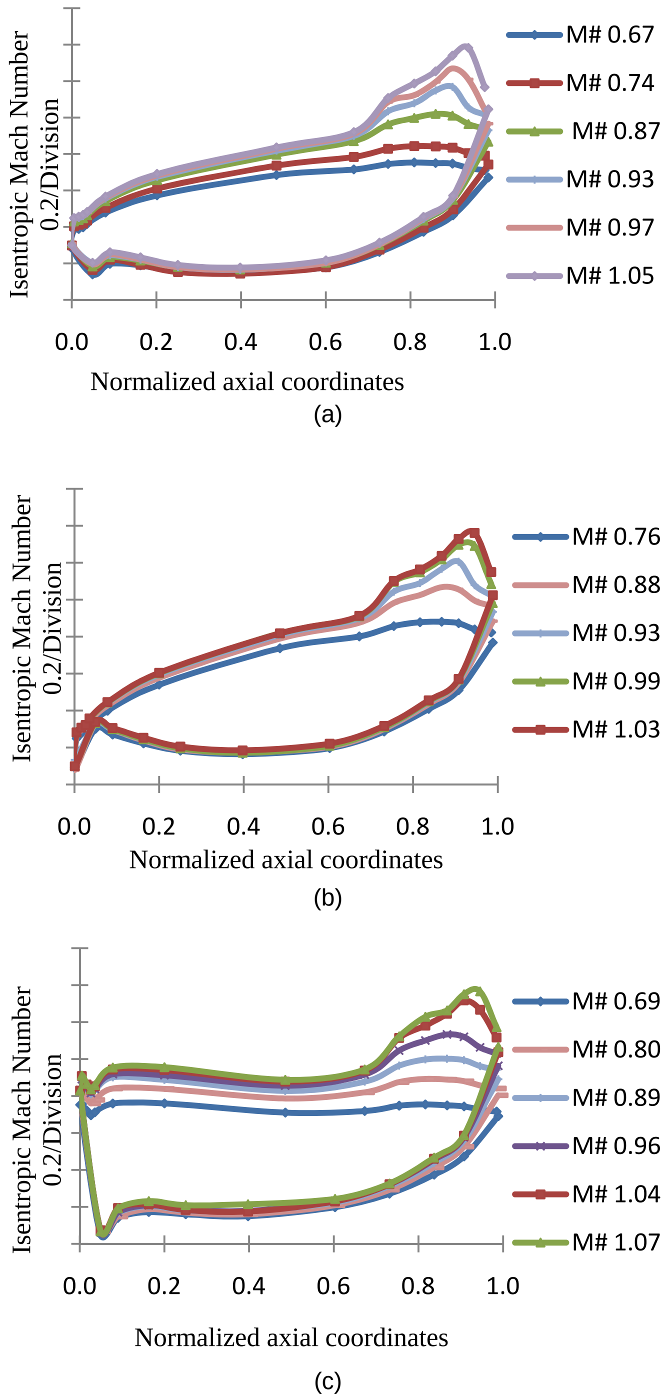

Figure 8: Effects of Mach number on airfoil loading at (a) design incidence (b) -10 deg off design incidence (c) +10 deg off design incidence for blade A (experimental data)

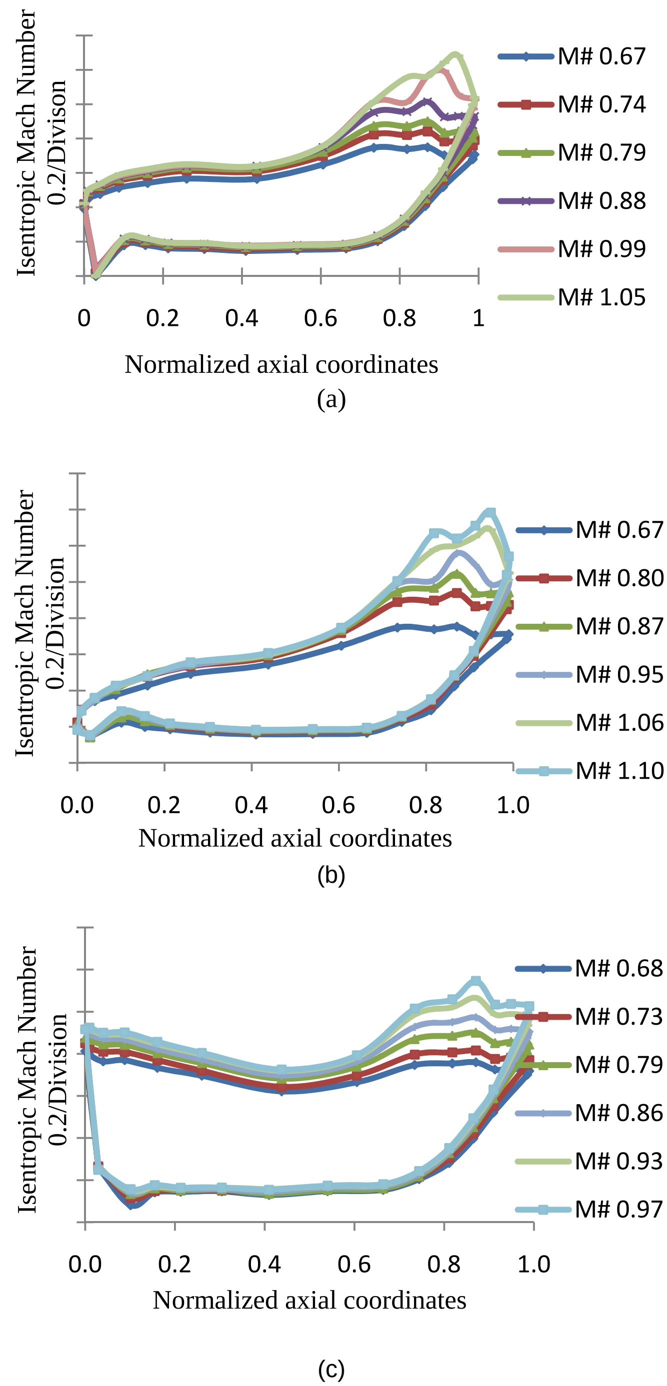

Figure 9: Effects of Mach number on airfoil loading at (a) design incidence (b) -10 deg off design incidence (c) +10 deg off design incidence for blade B (experimental data)

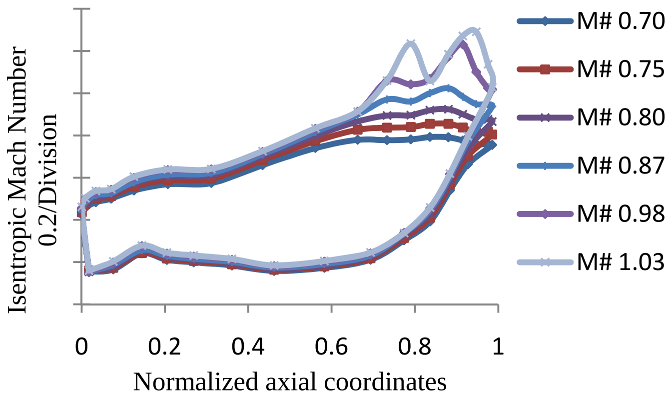

(a)

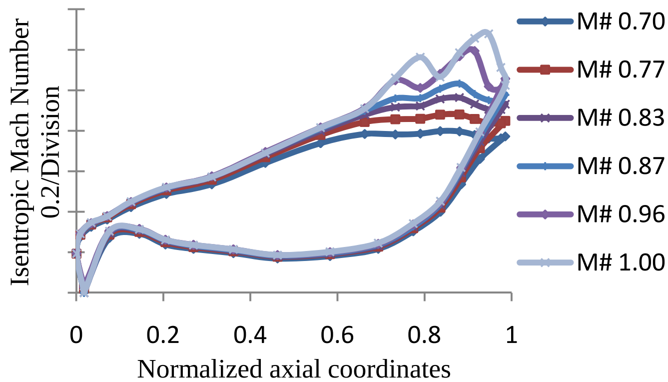

(b)

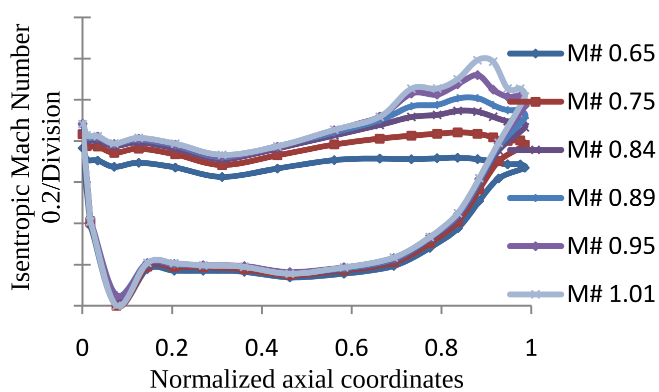

(c)

Figure 10: Effects of Mach number on airfoil loading at (a) design incidence (b) -10 deg off design incidence (c) +10 deg off design incidence for blade C (experimental data)

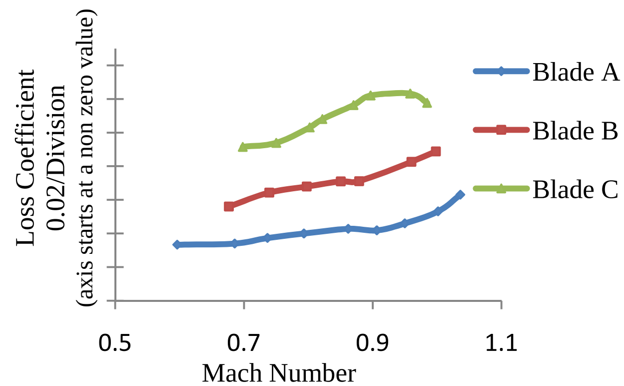

(a)

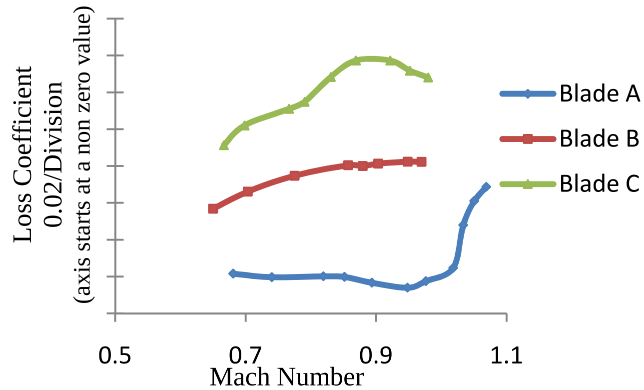

(b)

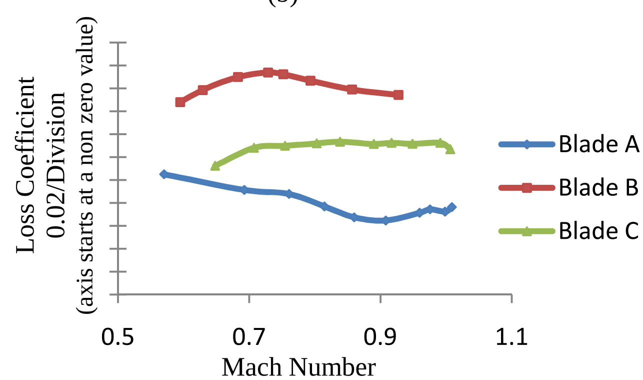

(c)

Figure 11: Loss coefficient measurements as a function of exit Mach number, based on measurements 1.0 axial chord downstream at (a) design incidence (b) -10 deg off design incidence (c) +10 deg off design incidence (experimental data)

For the +10 degree cases, the losses are higher than the other two incidence angle cases for all three airfoils. The rise in losses is due to the increased loss production in the suction side boundary layer on the frontward part of the airfoil as discussed previously using the vorticity plots (Figure 7). A comprehensive study on the effect of varying incidence angles on downstream losses was done by Abraham et al. [11].

Secondary Losses:

Secondary losses arise from secondary flows which are always present when a wall boundary layer is turned through an angle by an adjacent curved surface. Figure 12 shows the pitchwise area averaged losses measured at various spanwise locations 1.0 axial chord downstream from the trailing edge of the cascade at the design exit Mach number and at the design incidence angle. The spanwise measurements were taken during multiple runs with a traversing kiel probe from midspan to inclined endwall. Regions of higher losses are clearly visible near the end walls and are a result of complex vortices arising due to the secondary flows. Pressure gradients in the passage caused by the boundary layer velocity distribution and flow stagnation on the airfoil result in the creation of secondary flows in the end wall region. These pressure variations force the flows toward the end wall and also lead to the development of two legs of the leading edge vortex. The turning angle of the flow between the airfoils results in the creation of a strong pressure gradient across the passage. This gradient influences the paths of the two legs of the horseshoe vortex and also the low velocity flow near the end wall. The pressure side leg of the horseshoe vortex which is forced to flow in a downward direction, towards the suction side of the passage, combines with the low velocity flow near the end wall and forms the passage vortex. The passage vortex drifts from the pressure side leading edge toward the suction side trailing edge of the adjacent airfoil. As this vortex approaches the suction side, it lifts off the end wall, adheres along the suction side and moves downstream in the passage. At the same time the suction side horseshoe vortex remains close to the end wall until it meets the passage vortex. It then wraps itself around the passage vortex instead of adhering to the suction surface, lifts off the end wall and continues downstream along the suction side. This vortex is identified in Figure 12 by a region of high losses as compared to midspan losses. This region varies for the three airfoils from a normalized span around 0.70 to 0.85 in the experimental results. A fair agreement is observed between CFD and experimental regions, especially for the blades A and C. The CFD results show prominent high loss region from 0.7 to 0.85 normalized span due to secondary vortex flow, whereas this region in experimental data is quite diffused 1 Cax downstream of the trailing edge. The loss levels of the three airfoils obtained from CFD show that loss for airfoil A is less than those for airfoil B, which is less than those for airfoil C. This trend is similar to the results obtained from experiments. Airfoil A shows comparatively lower losses along the entire span. The losses due to secondary flows appear closer to the endwall for Blade C as compared to the other airfoils. However, the CFD predictions show almost equal and a much steeper loss gradient near the end wall. The overall area averaged losses obtained from experiments by taking the average of the pitchwise and spanwise losses at design condition are plotted in Figure 13. Airfoil A shows the lowest overall losses, which is consistent with all of the previous analysis while airfoils B and C exhibit higher (by almost 29%) and similar overall loss levels.

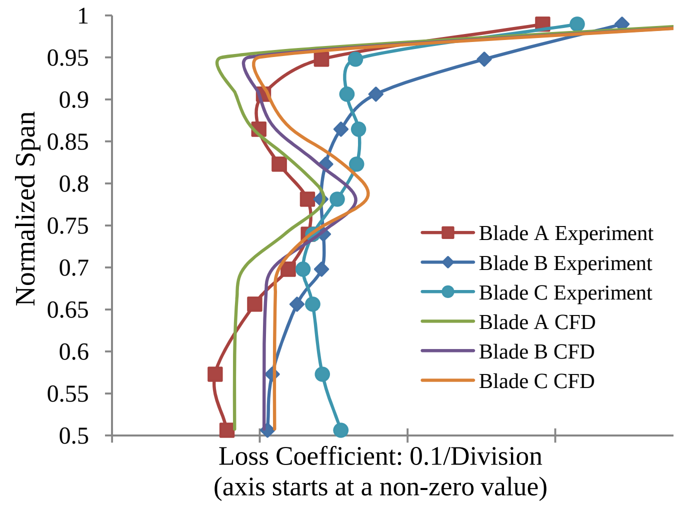

Figure 12: Spanwise Loss Variation at design condition

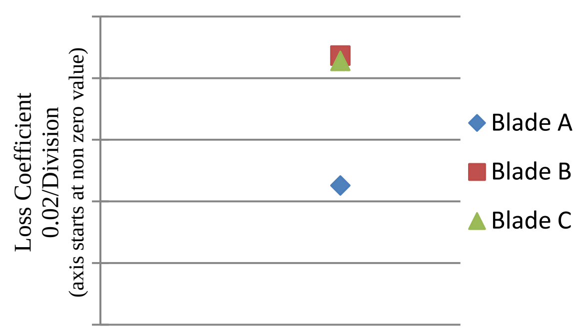

Figure 13: Area averaged losses at design condition
(experimental data)

CONCLUSIONS

One of the goals of this study is to use the data to confirm/refine loss predictions for the effect of various Mach numbers and gas turning. Loss systems provide predictions for pressure loss as the various geometric and aerodynamic parameters are varied. Airfoils are then designed to produce the target velocity triangles. In this study experimental measurements and numerical predictions for a high turning, high loading turbine airfoil have been carried out at design and off design conditions in a linear transonic cascade wind tunnel.

The effect of variation of exit Mach number on airfoil loading is felt mainly toward the trailing edge region of airfoil and the loading at the leading edge remains almost the same for different Mach numbers. The airfoil loading results from experiment and CFD analysis agree reasonably well.

By studying the airfoil loading at different conditions and the corresponding loss levels, we can conclude that the losses are prominently governed by three physical phenomena. With higher aft diffusion, flow separation on the rear part of the suction surface of the airfoil occurs, which leads to higher losses. Shocks originating from the trailing edge of the adjacent airfoil and impinging on the rear of the airfoil suction surface affect losses adversely. Flow separation on the frontward suction side, as seen at high incidence angle cases, plays a major role in higher loss production.

ACKNOWLEDGEMENTS

The authors are grateful to the help and support provided by Song Xue at Virginia Tech. The permission for publication by Siemens Energy and their technical support is gratefully acknowledged by the authors.

REFERENCES

[1] Prakash, C., Cherry, D. G., Shin, H. W., Machnaim, J., Dailey, L., Beacock, R., Halstead, D., Wadia, A. R., Guillot, S. and Ng, W. F., "Effect of Loading Level and Distribution on LPT Losses," *ASME Paper* GT2008-50052, 2008.

[2] Corriveau, D., and Sjolander, S. A., 2004, "Influence of Loading Distribution on the Performance of Transonic HP Turbine Blades," ASME J. Turbomach., 126, pp. 288–296.

[3] Funazaki, K., Takahiro, S. and Haruyuki, T., "Effects of Blade Loading Distribution on Aerodynamic Performance of Ultra-High Lift LP Turbine Airfoils Under the Influences of Wake Passing and Freestream Turbulence", ASME paper GT-2010-22134.

[4] Popovic, I., Zhu, J., Dai, W., Sjolander, S. A., Praisner, T. and Grover, E., "Aerodynamics of a Family of Three Highly Loaded Low-Pressure Turbine Airfoils: Measured Effects of Reynolds Number and Turbulence Intensity in Steady Flow", ASME paper GT-2006-91271.

[5] Zoric, T., Popovic, I., Sjolander, S. A., Praisner, T. and Grover, E., "Comparative Investigation of Three Highly Loaded LP Turbine Airfoils: Part I – Measured Profile and Secondary Losses at Design Incidence", ASME paper GT-2007-27537.

[6] Zoric, T., Popovic, I., Sjolander, S. A., Praisner, T. and Grover, E., "Comparative Investigation of Three Highly Loaded LP Turbine Airfoils: Part I – Measured Profile and Secondary Losses at Off-Design Incidence", ASME paper GT- 2007-27538.

[7] Benner, M. W., Sjolander, S. A., and Moustapha, S. H., 2004, "The Influence of Leading Edge Geometry on Secondary Losses in a Turbine Cascades at the Design Incidence," ASME J. Turbomach., **126**, pp. 277–287.

[8] Maclsaac, G.D., Sjolander, S.A. and Praisner, T.J., 2010, "Measurements of Losses and Reynolds Stresses in the Secondary Flow Downstream of a Low Speed Linear Turbine Cascade," ASME paper GT2010-22727.

[9] Jouini, D. B. M., Sjolander, S. A., and Moustapha, S. H., 2001, "Aerodynamic Performance of a Transonic Turbine Cascade at Off-Design Conditions," ASME J. Turbomach., 123, pp. 510–518.

[10] Jouini, D. B. M., Sjolander, S. A., and Moustapha, S. H., 2002, "Midspan Flow-Field Measurements for Two Tran-Sonic Linear Turbine Cascades at Off-Design Conditions," ASME J. Turbomach., 124, pp. 176–186.

[11] Abraham, S., Panchal, K., Xue, S., Ekkad, S.V., Ng, W., Malandra, A. and Brown, B.J., 2010, "Experimental and Numerical Investigations of a Transonic High Turning Turbine Cascade with a Divergent Endwall," FEDSM paper FEDSM-ICNMM2010-30393.

[12] Taremi, F., Sjolander, S.A. and Praisner, T.J., 2010, "Measurements of Endwall Flows in Transonic Linear Turbine Cascades: Part I Low Flow Turning," ASME paper GT2010-22759.

[13] Taremi, F., Sjolander, S.A. and Praisner, T.J., 2010, "Measurements of Endwall Flows in Transonic Linear Turbine Cascades: Part II High Flow Turning," ASME paper GT2010-22760.

[14] Praisner, T. J. and Clark, J. P., "Predicting Transition in Turbomachinery, Part I – A Review and New Model Development", ASME paper GT-2004-54108.

[15] Praisner, T. J., Grover, E. A., Rice, M. J. and Clark, J. P., "Predicting Transition in Turbomachinery, Part II – Model Validation and Benchmarking", ASME paper GT-2004-54109.

[16] Menter, F. R., Langtry, R. B., Likki, S. R., Suzen, Y. B., Huang, P. G., "A Correlation-Based Transition Model Using Local Variables: Part I – Model Formulation", ASME GT-2004-53452.

[17] Langtry, R. B., Menter, F. R., Likki, S. R., Suzen, Y. B., Huang, P. G., "A Correlation-Based Transition Model Using Local Variables: Part II – Test Cases and Industrial Applications", ASME GT-2004-53454.

[18] Nagel, M. G., and Baier, R.-D., 2005, "Experimentally Verified Numerical Optimization of a Three-Dimensional Parametrized Turbine Vane With Nonaxisymmetric End Walls," ASME J. Turbomach., 127, pp. 380–387.

[19] Gregory-Smith, D. G., and Cleak, J. G. E., 1992, "Secondary Flow Measurements in a Turbine Cascade with High Inlet Turbulence," ASME J. Turbomach., **114**, pp. 173–183.

